Structure of the runaway electron loss during induced disruptions in TEXTOR

K. Wongrach, K. H. Finken, S. S. Abdullaev, O. Willi, L. Zeng, and Y. Xu

Citation: Physics of Plasmas **22**, 102508 (2015); doi: 10.1063/1.4933131
View online: http://dx.doi.org/10.1063/1.4933131
View Table of Contents: http://scitation.aip.org/content/aip/journal/pop/22/10?ver=pdfcov
Published by the AIP Publishing

Structure of the runaway electron loss during induced disruptions in TEXTOR

K. Wongrach,[1] K. H. Finken,[1] S. S. Abdullaev,[2] O. Willi,[1] L. Zeng,[3] and Y. Xu[4]
[1]*Institut für Laser- und Plasmaphysik, Heinrich-Heine Universität Düsseldorf, Düsseldorf 40225, Germany*
[2]*Institut für Energie- und Klimaforschung, Forschungszentrum Jülich GmbH, Jülich 52428, Germany*
[3]*Institute of Plasma Physics, Chinese Academy of Sciences, Hefei, Anhui 230031, People's Republic of China*
[4]*Southwestern Institute of Physics, Chengdu 610041, People's Republic of China*

(Received 12 March 2015; accepted 1 October 2015; published online 15 October 2015)

The loss of runaway electrons during an induced disruption is recorded by a synchrotron imaging technique using a fast infrared CCD camera. The loss is predominantly diffuse. During the "spiky-loss phase", when the runaway beam moves close to the wall, a narrow channel between the runaway column and a scintillator probe is formed and lasts until the runaway beam is terminated. In some cases, the processed images show a stripe pattern at the plasma edge. A comparison between the MHD dominated disruptions and the MHD-free disruption is performed. A new mechanism of plasma disruptions with the runaway electron generation and a novel model which reproduces many characteristic features of the plasma beam evolution during a disruption is briefly described.
 [http://dx.doi.org/10.1063/1.4933131]

I. INTRODUCTION

In the development of fusion based on tokamaks, runaway electrons (REs) generated during disruptions are of major concern as they travel with high velocities that exceed the friction force and can be freely accelerated. In the present tokamaks, REs can gain energies up to several tens of MeV. The high energy electrons may cause severe damage to the vessel walls and other components inside the torus. This problem becomes more important, e.g., in ITER because runaways with energies up to ~100 MeV are expected.[1] However, the REs with energies of the order of 10 MeV become dominant when the avalanching commences.[2] Studies of REs generated during disruptions have been performed at nearly all major tokamaks. The toroidal magnetic field plays an important role in runaway generation. No REs are observed for disruptions when the magnetic field is below the magnetic threshold.[3,4] With decreasing magnetic field, the level of magnetic fluctuation increases.[5] In the presence of micromagnetic turbulence and low m/n mode magnetic islands in stochastic sea, REs are better confined than the thermal electrons. Macroscale magnetic turbulence, conversely, degrades the runaway confinement.[6] In DIII-D, the runaway current depends critically on MHD fluctuations, particularly the radial profile of the $n = 1$ mode.[7]

Disruptions with a substantial runaway population show at first a rapid decay of the plasma current followed by a plateau like formation with a reduced decay rate. During the first strong decay phase, the loop voltage is enhanced acting as the driving force for the REs. In addition to the continuous decay during the plateau phase, a small stepwise decays of the plasma current and loss spikes accompanied by MHD activity are observed.[8] The main emphasis of this article is laid on an imaging of the plasma cross section by the synchrotron radiation measurement in order to provide a better understanding of the mechanism behind the loss. We also try to show similarities and differences between the observations during the runaway plateau phase of two different groups of disruptions.

II. EXPERIMENTAL SETUP

A CCD IR-camera has been installed at the low field side of the torus oriented tangentially in the electron approach direction and has been used to record images of synchrotron radiation emitted by high energy REs (see Figure 1). The camera is sensitive only to electrons which have energies exceeding 25 MeV with an instantaneous velocity vector in the direction of the camera entrance optics. This restricts the synchrotron image to a narrow area[9] with a toroidal integration length of about 10 cm. As the field of observation of the plasma at the high field side is vignetted, the camera detects only synchrotron radiation emitted by REs at the low field side. The camera is operated at a frame rate of 1253 frames

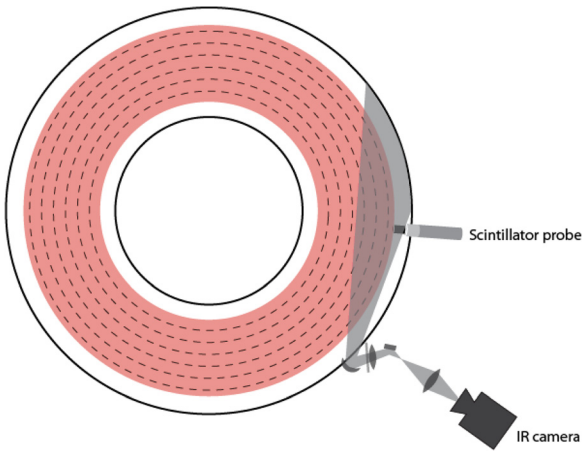

FIG. 1. Schematic top view of experimental setup. Solid black lines indicate the vacuum chamber wall. A gray area represents the field of view of the IR camera. The scintillator probe is placed at the last closed flux surface.

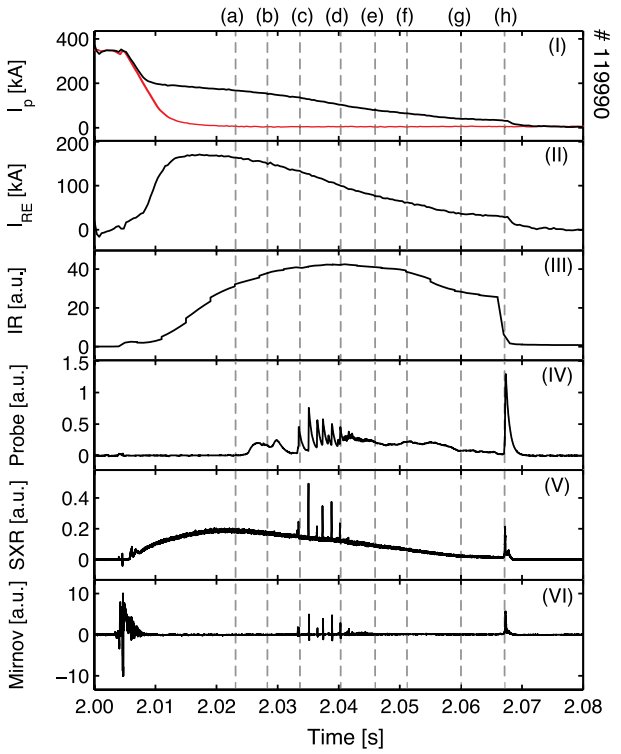

FIG. 2. Temporal evolution of the disruption of the discharge No. 119990 (top to bottom): (I) time trace of the plasma current (black curve) and of the current without REs (red curve), (II) the runaway current, (III) the spatially integrated synchrotron radiation, (IV) the scintillator probe signal for REs with energies above 11 MeV, (V) the soft X-ray signal, and (VI) the Mirnov signal.

per second, corresponding to the time distance between consecutive images of 0.8 ms, with an integration time of 2 μs.

The REs at the plasma edge are measured by the scintillator probe,[10] which is placed at the last closed flux surface ($r = 46$ cm) shortly before the disruption is triggered. The probe consists of 9 scintillating YSO crystals, which are partially shielded by layers of stainless steel of different thickness; therefore, they are sensitive to REs with different energies from 3 MeV to about 22 MeV. The probe is covered by a 5 mm thick carbon fibre composite (CFC) mantle such that neither light nor electrons with energies below 3 MeV can hit the scintillator crystals. During the pre-programmed disruptions, the radial position control coils are operated in a feed-forward mode.

At TEXTOR, reproducible disruptions with REs can be initiated by a fast injection of argon gas.[11–13] The disruptions reported in this paper are induced by argon injection at $t = 2$ s performed by a fast valve. The discharge conditions are: a stationary, ohmic discharge with circular cross section at a major radius of $R_0 = 1.75$ m, and a minor radius of $a = 0.46$ m. The plasma current is $I_p = 350$ kA, the toroidal field strength is $B_T = 2.4$ T, and the line average density before the disruption is $n_e = 1.5 \times 10^{19}$ m^{-3}.

III. RUNAWAY LOSS DURING INDUCED DISRUPTION

Although the same conditions were applied to all disruptions in the recent experiments, two distinct groups of disruptions have been observed. The first group consists of a MHD-dominated plateau phase, during which the MHD activity is observed. The other group, the MHD-free runaway disruption, has a smooth runaway plateau phase. Neither runaway bursts nor soft X-ray (SXR) and Mirnov signal spikes are present. The existence of the spikes is independent of the presence of the scintillator probe near the plasma edge.

A. MHD-dominated plateau phase

A typical example of an induced disruption with MHD activity in the TEXTOR tokamak is shown in Fig. 2. The current plateau as seen in the first sub-figure (black curve) typically indicates the presence of REs. In the discharge without runaways, one observes only the exponential decay (red curve). The second sub-figure shows the difference between the current traces with and without REs and thus gives the pure contribution of the runaways to the plasma current. The plateau phase of the current is initially flat until the spiky bursts are present between $t = 2.032$ s and $t = 2.045$ s. The spikes are observed in the probe, the SXR, and the Mirnov signals at the same time. However, the amplitudes of the spikes are different indicating that the spikes are probably local and not uniform around the torus. The integrated synchrotron signal starts to increase after a delay with respect to the runaway current because the synchrotron measuring system is sensitive to the electrons with energies above 25 MeV. The integrated synchrotron signal increases until the spiky loss starts. Afterwards, it decays smoothly. At the end, we observe a sudden loss of the synchrotron radiation.

In Fig. 3, a compilation of images of the synchrotron light recorded in the discharge No. 119990 is shown in false color. As already mentioned, the images show a cross section of the high energy runaway beam. The left side of the images represents the high field side which is partially vignetted. Therefore, one cannot see the radial extend of the runaways in the first frames of the disruption. Later, the runaway beam

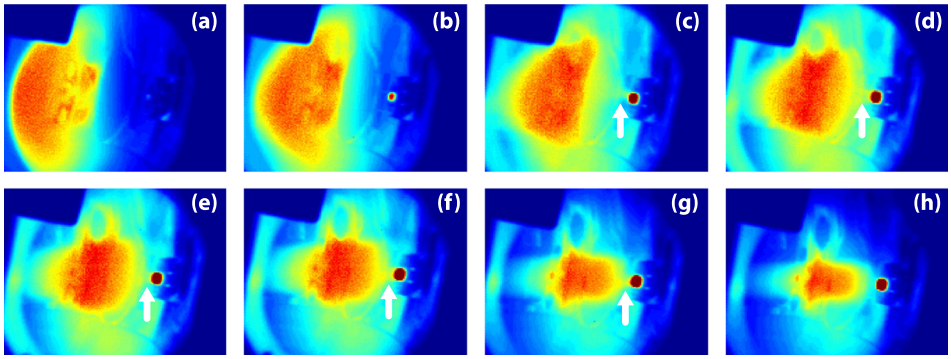

FIG. 3. Temporal evolution of IR radiation patterns of the discharge No. 119990 taken at (a) $t = 2.023$ s, (b) $t = 2.028$ s, (c) $t = 2.033$ s, (d) $t = 2.040$ s, (e) $t = 2.046$ s, (f) $t = 2.051$ s, (g) $t = 2.060$ s, and (h) $t = 2.068$ s. A small red spot at the right side of the image represents the heated scintillator probe tip. The white arrows in sub-figures (c)–(g) indicate the channel between the core runaways and the probe tip.

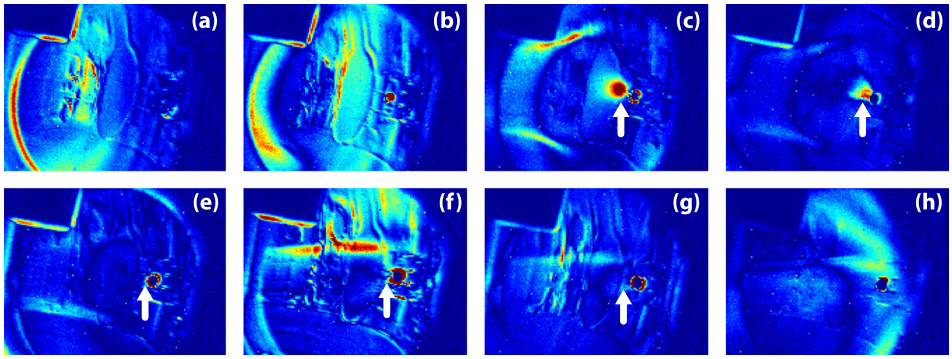

FIG. 4. The images obtained from subtracting consecutive images of the discharge No. 119990 corresponding to the images shown in Fig. 3. In sub-figures (c) and (d), i.e., at the time of the MHD spikes, the channel is clearly visible. The white arrows in sub-figures (c)–(g) indicate the position of the channel between the core runaways and the probe tip.

is shifted more towards the low field side allowing the whole beam to be seen. The runaway column is spatially rather smooth and has a circular shape. The radius of the runaways is about 20 cm. The "horn like" double structure which one sees on the upper part of the image is an artifact from reflections of the wall (from the stiffening ring at a window). The IR structure remains fixed in space. At the low field side, one sees a small red dot at the edge of the runaway beam. This dot is the tip of the scintillator probe which is heated by the lost REs and runaway halo. Later in the disruption, when the plasma current is already low, the runaway beam shrinks and takes an oval shape oriented horizontally before it suddenly disappears at the end of the discharge, i.e., within 80 μs.

To our surprise, we did not observe special structures in the runaway beam during the spiky phase but a rather diffuse loss. Nevertheless, when the runaway beam is shifted close to the probe, a small channel which connects the runaway column to the probe is observed. The channel is formed at the beginning of the spiky phase and lasts until the runaway beam is terminated (see sub-figures (c)–(g)). However, there was no indication of fast variations during the individual spikes.

In order to detect weak local structures which vary in time, we have developed a technique to subtract each image from its previous image. This technique is close to a time derivative of the images or related to a stroboscopic method; it visualizes in particular events which are quickly developing. This technique enables an observation of the runaway beam structures, which change on the time scale of the image recording time. Fig. 4 shows the absolute values of the differences between the consecutive images related to the images shown in Fig. 3. The intensity of the color code is increased by a factor of 10. Sub-figure (a) shows an enhanced intensity because the number of high energy electrons is increasing. In sub-figure (b), an intensity of synchrotron radiation at the low field side increases due to an outwards movement of the beam. Sub-figures (c) and (d) are taken during the spiky phase. One sees that the influence zone of the probe is well restricted to few centimeters only and does not influence the central runaway population. Some narrow stripes at the top and bottom of the beam presented in sub-figure (c)–(e) may indicate an enhanced loss during the spikes.

B. MHD-free runaway disruptions

Fig. 5 shows an example of a "smooth" disruption with runaways. One sees only week signs of MHD activity. No SXR and Mirnov spikes are detected. The scintillator probe was absent during this experiment. A slow radial oscillation of the runaway beam results in the variations of the IR signal and the plasma current.

The image of the synchrotron radiation is not spectacular and develops slowly. Therefore, we have selected only 4 images (see Fig. 6). The radius of the runaway beam in this example is 26 cm. It is larger than the radius in the previous example. No loss channel connecting between the runaway beam and wall elements is observed. The images obtained from subtracting consecutive images shown in Fig. 7 are surprising. We find, after a smooth beginning phase, the development of a stripe pattern at the edge of the runaway column. The stripes are inclined with respect to the expected magnetic flux surfaces. Inclinations in both directions as well as a superposition of the stripes are observed at the edge of the beam.

C. Comparison of runaways with and without MHD activity

The plasma current of a discharge without MHD activity (black) in comparison with that of a discharge with MHD

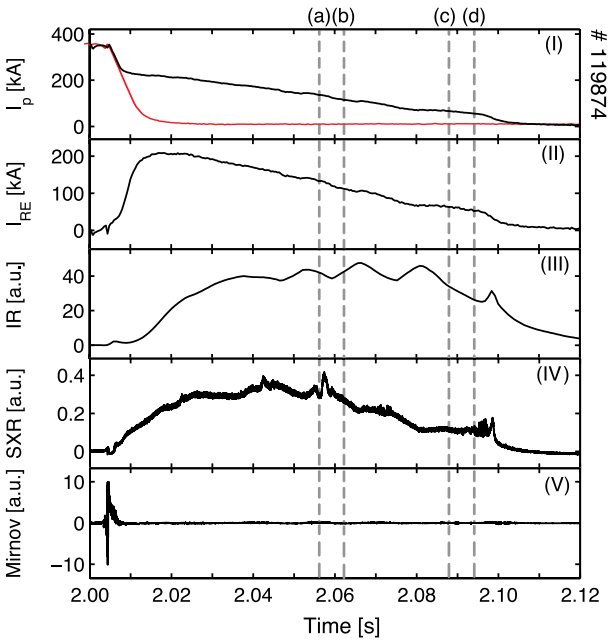

FIG. 5. Temporal evolution of the disruption of the discharge No. 119874 (top to bottom): (I) time trace of the plasma current (black curve) and of the current without runaway electrons (red curve), (II) the runaway current, (III) the spatially integrated synchrotron radiation, (IV) the soft X-ray signal, and (V) the Mirnov signal.

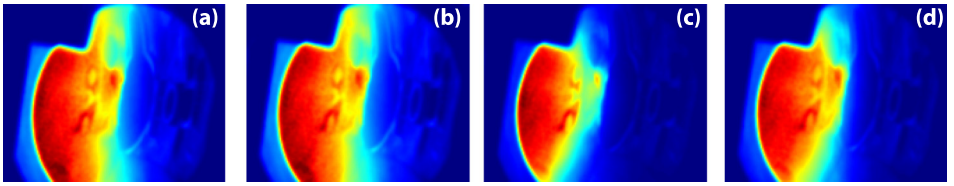

FIG. 6. Temporal evolution of the IR radiation patterns of the discharge No. 119874 taken at (a) $t = 2.057$ s, (b) $t = 2.062$ s, (c) $t = 2.088$ s, and (d) $t = 2.093$ s. A small red spot at the right field side of the image presents the heated scintillator probe tip.

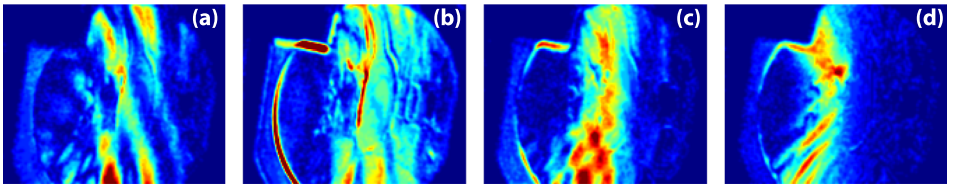

FIG. 7. The images obtained from subtracting consecutive images of the discharge No. 119874 corresponding to the images shown in Figure 6.

activity (red) is shown in Fig. 8. The current decay during the runaway plateau phase in case of discharge without MHD activity can be described by a linear function of time with a decay rate of 2.3 MA/s (see dashed blue line). In case of a discharge with MHD activity, the current starts to decrease with the same rate as the current in the previous case. However, during the spiky phase, the decay rate increases to 4.1 MA/s. The variation of the plasma current due to the slight movement of the beam is minor in comparison with the current drop during the spiky phase.

Although the runaway loss is substantially enhanced, no significant change of synchrotron radiation is observed. The major part of the high energy runaways remains confined in the plasma as can be seen in Figs. 3(c)–3(e) and 4(c)–4(e). The lost runaways are mainly the REs in low and energy range. This is consistent with the earlier publication,[8] in which the energy spectrum of the lost RE was analyzed by the different channel of the scintillator probe. The spectrum of the lost runaways was described by an exponential decay function with an exponent of $n_{r_0} \sim 10$ MeV. At that time, the probe was well calibrated. At present, the calibration is old and no longer reliable because the probe housing was modified.

It has been observed that runaway disruptions with MHD-activity often show channels between the main runaway beam and the probe or other wall elements. During runaway disruptions without MHD-activity, we have never seen those channels even when the beam moves close to the probe and the probe is continuously heated by the beam halo. However, it has to be stated that these channels are not visible in all spiky disruptions, probably because they are out of sight of the IR-camera. There are disruptions, during which the spikes are present when the runaway beam moves toward the wall at the HFS. The loss channel connecting between the wall and the beam is probably created. But this part is located outside the camera field of view. We, therefore, cannot see whether the channels exist or not.

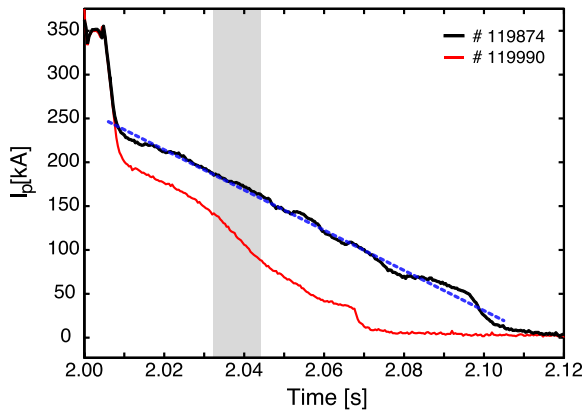

FIG. 8. The plasma current of the discharges No. 119874 (black–quiet disruption) and No. 119990 (red–spiky disruption). A dashed blue line represents a linear fit of the current of the discharges No. 119874. A gray area indicates the spiky phase.

During some smooth disruptions, the stripe structure likes in Fig. 7 has been observed. In runaway disruptions with MHD-activity, we have not yet seen these stripe patterns. It is still unclear, whether the stripe structure is systematically connected to MHD-free disruptions or whether it was just an accident that we found it only there. We suspect that the plasma rotation frequencies in case of spiky disruptions and smooth disruptions are different. The rotation frequency in the former case possibly does not match the recording frequency of the camera. The observed structures are smeared out, and hence the smooth runaway beam is detected.

IV. STRUCTURE OF RUNAWAY ELECTRON ORBITS

The stripes are a characteristic feature for an ergodic system and related to the so-called laminar zones.[14,15] To explain the observed stripes in synchrotron radiation patterns, we have created a model which describes practically topological features in the plasma. According to our assumptions, the most stable RE beams are created in plasmas with the central safety factor $q(0) < 1$.[16,17] They are formed in the central plasma region confined inside the intact magnetic surface located between the rational magnetic surface $q = 1$ and the closest low-order rational magnetic surface $q = 5/4$ (or $q = 4/3,\ldots$). Heat and plasma particles outside this region are lost due to transport in a strong stochastic magnetic field formed due to nonlinearly excited low-mode number MHD modes. Electrons in the confined region are accelerated by the inductive toroidal electric field.

Based on the new model, REs are mainly lost due to two effects. The smooth decay of RE current is related to the outward drift of electron orbits induced by a toroidal electric field.[18,19] This loss mechanism plays an important role for high energy REs, since they have large drift orbit displacement. The

sudden losses of REs are caused by the nonlinear interactions of high energy runaway orbits with the $m/n = 1/1$ helical magnetic perturbation leading to the formation of stochastic layer of REs at the beam edge. The typical Poincaré section of RE orbits in the presence of the $m/n = 1/1$ mode is shown in Fig. 9. The presence of the ergodic layer is consistent with the observation that the runaway beam fills only about one half of the predisruptive plasma diameter, while one sees a larger runaway beam in typical low density runaway discharges.[9] In Fig. 9, mixed topological structures are observed: the large intact area inside the $q = 1$ surface and a series of stable islands embedded into a stochastic layer near the separatrix that open to the wall. The high energy REs are less sensitive to the magnetic turbulence due to their strong drift.[20] Therefore, the lost REs are mainly from the low energy range. The characteristic escape time of REs from the stochastic layer is of order of 10 μs. However, REs trapped inside the islands stay longer and their synchrotron radiation can be seen. Due to the rotation of the $m/n = 1/1$ helical magnetic perturbation, the islands also rotate. This can explain the observed stripes in subtracted synchrotron radiation patterns.

V. SUMMARY AND CONCLUSIONS

During TEXTOR disruptions, REs and in particular, their loss have been measured—besides by the standard diagnostics—by synchrotron radiation imaging and by a scintillator probe positioned close to the plasma edge. The synchrotron radiation in the observed wavelength range is emitted from REs with energies exceeding 25 MeV while scintillator probe is most sensitive for electron energies in the range of 3 MeV to 22 MeV. REs with energies below 3 MeV as well as low energy particles are stopped by a CFC light tight mantle beyond the probe head.

The disruptions are initiated by massive injection of Ar-gas and the initial conditions are constant. In nearly all cases after the thermal quench, the development of a runaway plateau is observed. In the plateau phase, we distinguish the case with MHD-activity in the form of short spikes and the case of MHD-free plateau phase. One aim of the investigations by the synchrotron imaging is to find special "structures" in the runaway beam which are responsible for the MHD-spikes. As a result, a channel between the runaway beam and the probe head is identified. However, MHD activity is also present, although the probe is not applied and no channel is detected. The loss is best described as a diffusive loss.

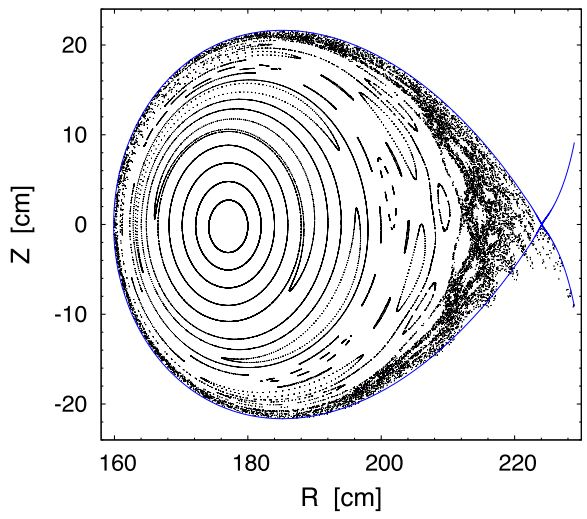

FIG. 9. Poincaré section of the RE guiding center. The RE energy $E = 20$ MeV and he RE beam current of $I_p = 100$ kA.

Without MHD activity, the loss is again best described as a diffusive process. However, by a special synchrotron image subtraction method, we find stripe-structures which resemble the laminar zone of an open ergodic system. The observed stripes in the subtracted IR-pictures may result from the rotation of the mixed topological structure of the stochastic layer created by the resonant interactions of high energy RE orbits with the $m/n = 1/1$ helical magnetic perturbation.

The observation of the laminar pattern leads to the development of a model, which explains many of the observed features: During the energy quench, low m/n modes are created including $m/n = 1/1$ and $m/n = 5/4$ (or 4/3). The REs generated in the large islands of those modes survive; this model explains the size of the runaway column of roughly one half of the pre-disruptive plasma size, the diffusive loss of the runaways, the current decay rate of the plasma current, and also the development of the MHD spikes as an interaction of the runaways with the background modes.

ACKNOWLEDGMENTS

This work was supported by the Royal Thai Government, a Jülich R&D contract, the Trilateral Euregio Cluster (TEC), and the DFG program GRK 1203. The authors would like to thank Dr. H. R. Koslowski, M. Forster, M. Rack, Dr. O. Schmitz, and TEXTOR Team for their support.

[1]J. R. Martiín-Solís, B. Esposito, R. Sánchez, and J. D. Alvarez, Phys. Plasmas **6**, 238 (1999).
[2]G. Papp, M. Drevlak, T. Fülöp, P. Helander, and G. I. Pokol, Plasma Phys. Controlled Fusion **53**, 095004 (2011).
[3]R. D. Gill, B. Alper, M. de Baar, T. C. Hender, M. F. Johnson, V. Riccardo, and contributors to the EFDA-JET Workprogramme, Nucl. Fusion **42**, 1039 (2002).
[4]M. Lehnen, S. S. Abdullaev, G. Arnoux, S. A. Bozhenkov, M. W. Jakubowski, R. Jaspers, V. V. Plyusnin, V. Riccardo, U. Samm, JET EFDA Contributors, and TEXTOR Team, J. Nucl. Mater. **390–391**, 740 (2009).
[5]T. Kudyakov, S. S. Abdullaev, S. A. Bozhenkov, K. H. Finken, M. W. Jakubowski, M. Lehnen, G. Sewell, O. Willi, Y. Xu, and TEXTOR Team, Nucl. Fusion **52**, 023025 (2012).
[6]R. Yoshino and S. Takuda, Nucl. Fusion **40**, 1293 (2000).
[7]V. A. Izzo, D. A. Humphreys, and M. Kornbluth, Plasma Phys. Controlled Fusion **54**, 095002 (2012).
[8]M. Forster, K. H. Finken, T. Kudyakov, M. Lehnen, O. Willi, Y. Xu, L. Zeng, and TEXTOR Team, Phys. Plasmas **19**, 092513 (2012).
[9]K. H. Finken, J. G. Watkins, D. Rusbüldt, W. J. Corbett, K. H. Dippel, D. M. Goebel, and R. A. Moyer, Nucl. Fusion **30**, 859 (1990).
[10]T. Kudyakov, A. Jochmann, K. Zeil, S. Kraft, K. H. Finken, U. Schramm, and O. Willi, Rev. Sci. Instrum. **80**, 076106 (2009).
[11]S. A. Bozhenkov, M. Lehnen, K. H. Finken, M. W. Jakubowski, R. C. Wolf, R. Jaspers, M. Kantor, O. V. Marchuk, E. Uzgel, G. Van Wassenhove, O. Zimmermann, D. Reiter, and TEXTOR Team, Plasma Phys. Controlled Fusion **50**, 105007 (2008).

[12]M. Lehnen, S. A. Bozhenkov, S. S. Abdullaev, and M. W. Jakubowski, Phys. Rev. Lett. **100**, 255003 (2008).
[13]A. Savtchkov, K. H. Finken, and G. Mank, Rev. Sci. Instrum. **73**, 3490 (2002).
[14]K. H. Finken, S. S. Abdullaev, M. Jakubowski, R. Jaspers, M. Lehnen, and O. Zimmermann, Nucl. Fusion **46**, S139 (2006).
[15]S. S. Abdullaev, *Magnetic Stochasticity in Magnetically Confined Fusion Plasmas* (Springer, Cham, 2014).
[16]S. S. Abdullaev, K. H. Finken, K. Wongrach, M. Tokar, H. R. Koslowski, O. Willi, L. Zeng, and TEXTOR Team, Phys. Plasmas **22**, 040704 (2015).
[17]S. S. Abdullaev, K. H. Finken, K. Wongrach, M. Tokar, H. R. Koslowski, O. Willi, L. Zeng, and TEXTOR Team, J. Plasma Phys. **81**, 475810501 (2015).
[18]X. Guan, H. Qin, and N. Fisch, Phys. Plasmas **17**, 092502 (2010).
[19]S. S. Abdullaev, Phys. Plasmas **22**, 030702 (2015).
[20]J. R. Myra and P. J. Catto, Phys. Fluids B **4**, 176 (1992).